Nonlin. Processes Geophys. Discuss., 1, 1133–1161, 2014
www.nonlin-processes-geophys-discuss.net/1/1133/2014/
doi:10.5194/npgd-1-1133-2014

Nonlinear Processes in Geophysics
Discussions
Open Access

Site effect classification based on microtremor data analysis using concentration–area fractal model

A. Adib[1], **P. Afzal**[1], **and K. Heydarzadeh**[2]

[1]Department of Mining Engineering, Faculty of Engineering, South Tehran Branch, Islamic Azad University, Tehran, Iran
[2]Zamin Kav Environmental & Geology Research Center, Tehran, Iran

Received: 24 April 2014 – Accepted: 4 July 2014 – Published: 22 July 2014

Correspondence to: A. Adib (adib@azad.ac.ir)

Published by Copernicus Publications on behalf of the European Geosciences Union & the American Geophysical Union.

Abstract

The aim of this study is to classify the site effect using concentration–area (*C–A*) fractal model in Meybod city, Central Iran, based on microtremor data analysis. Log–log plots of the frequency, amplification and vulnerability index (k-g) indicate a multifractal nature for the parameters in the area. The results obtained from the *C–A* fractal modeling reveal that proper soil types are located around the central city. The results derived via the fractal modeling were utilized to improve the Nogoshi's classification results in the Meybod city. The resulted categories are: (1) hard soil and weak rock with frequency of 6.2 to 8 Hz, (2) stiff soil with frequency of about 4.9 to 6.2 Hz, (3) moderately soft soil with the frequency of 2.4 to 4.9 Hz, and (4) soft soil with the frequency lower than 2.4 Hz.

1 Introduction

Site effect caused by an earthquake may vary significantly in a short distance. Seismic waves trapping phenomenon leads to amplify vibrations amplitudes that may increase hazards in sites with soft soil or topographic undulations. Theoretical analysis and observational data have illustrated that each site has a specific resonance frequency at which ground motion gets amplified (Bard, 2000; Mukhopadhyay and Bormann, 2004).

Microtremor data analysis is applied in the recognition of the soil layers, prediction of shear-wave velocity of the ground, and evaluation of the predominant period of the soil during earthquake events. It has been proved that measurement and analysis of microtremor data is an efficient and low-cost method of seismic hazard micro zonation (Kanai and Tanaka, 1954; AIJ, 1993; Mukhopadhyay and Bormann, 2004; Beroya et al., 2009). Microtremors are weak ground motions with amplitude between 1 and 10 µm which always exist and are mostly generated by natural processes. Since these motions change the site effects and these changes are representative of the soil

NPGD
1, 1133–1161, 2014

characteristics, microtremors analysis is used to obtain information about soil vibration properties of sites (Kamalian et al., 2008).

Some scientists believe that the microtremors are mostly formed by Love and Rayleigh waves (Akamatu, 1961). However, they could be composed of Longitudinal and Rayleigh waves (e.g. Douze et al., 1964). Allam (1969) proposed that microtremors could be composed of body and/or surface waves and thus, it is possible that they are originated from any wave.

Microtremors are also applied to calculate the amplifications of horizontal movements in the free surface during earthquake events (Nakamura, 1989). Fundamentally, the method expressed the spectral amplification of a surface layer which could be obtained by evaluation of the horizontal to vertical spectral ratio of recorded microtremors. The amplification factor was resulted by several refracted waves in effect of their incidence into layer boundary. Thus, associated Rayleigh wave of microtremor would be a noise and is removed during H/V process. Moreover, H/V ratios of simultaneously measured records on ground surface and bedrock represented constant maximum acceleration ratio. Since every station has different characteristics, the records of one earthquake in various sites will be different. In soft soil location underlying a hard rock, H/V spectral ratio illustrates a clear peak. These peaks are spatially and temporally stable and could be considered as a fundamental (resonance) frequency of the site (Duval et al., 1994; Duval, 1996). This method is used by many scientists in order to identify small scale seismic risks and prepare detailed data for urban seismic microzonation. Konno and Ohmachi (1998) carried out a complete study about Nakamura's approximation and developed the matter to investigate multi-layered systems which is known as HVSR method. It is obtained from numerical studies of horizontal geological deposits that if there would be large impedance differences between deposits and bedrock, local fundamental frequency could be well presented by HVSR method. However, comparison of HVSR peaks with standard spectral ratio shows that the actual site amplification cannot be estimated from the amplitudes of HVSR peaks (Bard, 1998; Gosar et al., 2008; Sesame, 2004).

NPGD
1, 1133–1161, 2014

Identification of ground types is a main issue in the seismic geotechnical studies as well as site selection. There are many site effect classifications based on dynamical ground characteristics such as frequency, period, alluvial thickness, and shear wave velocity. Nogoshi and Igarashi (1971) proposed one of the common classifications of site effects (Table 2).

Additionally, Komak Panah et al. (2002) presented a classification based on HVSR method in the eastern and central Iran. Both used fundamental frequency as a main factor (Tables 1 and 2).

Euclidean geometry recognizes geometrical shapes with an integer dimension; 1-D, 2-D, and 3-D. However, there are many other shapes or spatial objects whose dimensions cannot be mathematically explained by integers, but by real numbers or fractions. These spatial objects are called fractals. In abstract form, fractals describe complexity in data distribution by estimation of their fractal dimensions. Different geophysical and geochemical processes can be described based on differences in fractal dimensions obtained from analysis of relevant geophysical data. Fractal models which established by Mandelbrot (1983) were applied to objects that were too irregular to be described by ordinary Euclidean geometry (Davis, 2002; Evertz and Mandelbrot, 1992). Fractal theory has been practical to geophysical and geochemical exploration since late 1980s (e.g. Agterberg et al., 1996; Afzal et al., 2010, 2011, 2012, 2013; Cheng et al., 1994; Daneshvar et al., 2012; Sim et al., 1999; Turcotte, 1986). Cheng et al. (1994) proposed a concentration–area (C–A) fractal model based on the relationship of elemental distributions and occupied areas. This idea and premise provided a scientific tool to demonstrate that an empirical relationship between C–A exists in the geophysical and geochemical data (Afzal et al., 2010, 2012; Cheng et al., 1994; Cheng, 1999; Goncalves et al., 2001; Sim et al., 1999). Cheng et al. (1994) showed that there are various parameters which have a key role in spatial distributions of most of the elements for a given geological–geochemical environment.

In this paper, fundamental frequency, amplification and ground vulnerability index (k-g value) data of Meybod city (Central Iran) are separated by C–A fractal model and

NPGD
1, 1133–1161, 2014

Nogoshi's classification. Subsequently, results obtained by the both methods are compared.

2 Case study characteristics

Meybod city is located in the Yazd province, central Iran (Fig. 1), with Quaternary sediments as the major geological units (Fig. 2). Major types of the sediments are clay and silty clay. Additionally, sandy clay units occurred in the northeast part of the city with 2 m thickness and deep as 30–32 m.

Based on the geotechnical studies of the region, dominant soil type is composed of clay and silt with high plasticity (Fig. 3). Additionally, there is not any major variation in the composition of sediment in the area, except for some variation of clay and silt contents in the eastern part (based on borehole data) (Fig. 3).

From the downhole data which are collected from 5 boreholes, the variations of P and S velocity ($m\,s^{-1}$) were calculated (Table 3). Shear wave velocity is between 560 and 725 $m\,s^{-1}$ in the depth of 42 m. the depth of seismic bedrock varies from 52 to 90 m which are calculated based on the velocity. This result shows that there are differences in soil hardness values within the area.

3 Methodology

Measured microtremor data were analyzed by Nakamura technique (HVSR: Nakamura, 1989) and using SESAME software, based on Fast Fourier Transform (FFT). The results were mapped by Inverse Distance Squared (IDS) method using Rockworks TM v.15 software package. The results are fundamental frequency, amplification and ground vulnerability index (k-g value); k-g value has obtained by Eq. (1) (Nakamura, 1996):

$$\text{k-g} = (A_0)^2 / F_0 \quad (1)$$

NPGD
1, 1133–1161, 2014

where F_0 and A_0 are predominant frequency and its amplification factor, and k-g is an index to indicate deformation easiness of measured points which is expected to be useful to detect weak points of the ground (Nakamura, 1997).

For instance, k-g values obtained in San Francisco Bay Area after the 1989 Loma-Prieta Earthquake are bigger than 20 at the sites where grounds were deformed significantly and very small at the sites with no damage (Nakamura et al., 1990). However, comparison between k-g values obtained before the earthquake in 1994 and the damage degrees show that places with large k-g values correspond to the sites with big damage. This suggests k-g values representing the vulnerability precisely (Nakamura, 1997).

Concentration–area fractal model

Cheng et al. (1994) proposed concentration–area (C–A) model, which may be used to define the geophysical background and anomalies. The model is in the following general form:

$$A(\rho \leq \upsilon) \propto \rho^{-a1}; \quad A(\rho \geq \upsilon) \propto \rho^{-a2} \tag{2}$$

where $A(\rho)$ is the area with concentration values (frequency, amplification and k-g in this study) greater than the contour value ρ; υ is the threshold; and $a1$ and $a2$ are characteristic exponents.

The frequency size distributions for islands, earthquakes, fragments, ore deposits and oil fields often confirm the Eq. (2) (Daneshvar Saein et al., 2012). The two approaches which were used to calculate $A(\rho)$ by Cheng et al. (1994) were: (1) the $A(\rho)$ is the area enclosed by contour level ρ on a variables' contour map resulting from interpolation of the original data using a weighted moving average method, and (2) the $A(\rho)$ are the values that are obtained by box-counting of original regional variables' values. The breaks between straight-line segments on C–A log–log plot and the corresponding values of ρ have been used as thresholds to separate geophysical values into various components, showing different causal factors, such as lithological and mineralogical

NPGD
1, 1133–1161, 2014

differences, geochemical and geophysical processes and mineralizing events (Lima et al., 2003; Afzal et al., 2010, 2012; Heidari et al., 2013).

Fractal models are often used to describe self-similar geometries, while multifractal models have been utilized to quantify patterns; same as geophysical data defined on sets which themselves can be fractals. Extension from geometry to field has considerably increased the applicability of fractal/multifractal modeling (Cheng, 2007). Multifractal theory could be interpreted as a theoretical framework that explains the power-law relationships between areas enclosing concentrations below a given threshold value and the actual concentrations itself. To demonstrate and prove that data distribution has a multifractal nature requires a rather extensive computation (Halsey et al., 1986; Evertsz and Mandelbrot, 1992). This method has several limitations such as accuracy problems, especially when the boundary effects on irregular geometrical data sets are involved (Agterberg et al., 1996; Goncalves, 2001; Cheng, 2007; Xie et al., 2010).

The *C*–*A* model seems to be equally applicable as well to all cases, which is probably rooted in the fact that geophysical distributions mostly satisfy the properties of a multifractal function. Some evidence prove that geophysical data distributions are fractal in nature and behavior (e.g. Bolviken et al., 1992; Turcotte, 1997; Gettings, 2005; Afzal et al., 2012; Daneshvar Saein et al., 2012).

This idea may provide and help the development of an alternative interpretation validation as well as useful methods to be applied to geophysical distributions analysis (Afzal, 2012). Various log-log plots between a geometrical character such as area, perimeter or volume and a geophysical quality parameter like geoelectrical data in fractal methods are appropriate for distinguishing geological recognition and populations' classification in geophysical data because threshold values can be identified and delineated as breakpoints in those plots (Daneshvar Saein et al., 2012).

NPGD
1, 1133–1161, 2014

4 Application of *C–A* model

Microtremor data are measured at 160 point in the study area (Fig. 1) using three channeled seismometer device (SL07, SARA Company, Italy). It has natural frequency of 2 Hz and natural attenuation of 0.7. This device has a three channeled digitizer of 24 bit, a central process unit (CPU) to save records and a GPS receiver. The data were recorded by sampling frequency of 200 Hz and the average recording time of 12 min at each station. At first, a mesh was overlapped on the city map to determine the recording points. Then, recording on every point was regularly performed. When any of recording points was not appropriate for recording (e.g. because of existence of tall buildings), the point location was slightly shifted to achieve a clear data. Moreover, if any point was approximate to a heavy traffic street, the data were recorded at midnight. During recording process, the device was located on a leveled ground and was balanced. Usually, 10 min is required for any microtremor recording to record the minimum 1 Hz frequency (WP12 Sesame project, 2004).

The obtained frequencies, amplifications and k-g values are illustrated as contour maps applying IDS interpolation method (Fig. 4). The areas with different frequencies can be visually distinguished in the map. The studied area was gridded by 20 m × 20 m cells. The evaluated values in cells were sorted out based on decreasing grades, and cumulative areas were calculated for grades. Eventually, log-log graphs were plotted to separate the different populations.

Distributions of the fundamental frequency, amplification and k-g data are multimodal which their mean values are 3.24 Hz, 2.14 and 2.91, respectively (Fig. 5). Variograms and anisotropic ellipsoids of the parameters were calculated to estimate data influence range of any point in order of plotting IDS maps (Fig. 6). These ellipsoids make the results estimated more accurate and we can determine the direction of the results variations. Based on the variograms and ellipsoids of the parameters, their major ranges have a W–E trend. It could be represented by the direction of soil variations that become more intense from west to the east of the area (Fig. 3).

NPGD
1, 1133–1161, 2014

According to the *C–A* log–log plots, four populations were distinguished for frequency and five populations for amplification and k-g reveals multifractal nature for the parameters in the Meybod city, as depicted in Fig. 7. Data distribution based on *C–A* model has been shown in Fig. 8. The sites with high intensity values of frequency are situated in the central parts of the area and the sites with high intensive amplification and k-g are located in the northern and eastern parts of the Meybod city.

The most part of the city has frequency lower than 4.9 Hz, especially between 2.4 to 4.9 Hz. The central part of the city is the only part with high frequency, as depicted in Fig. 8. It represents that it is more competent than the other parts. Based on the resulted frequencies, the most parts of the city contain soft soils, but amplification and k-g quantities are very low, lower than 2.4 and 4.2, respectively.

5 Comparison between Nogoshi classification and fractal modeling results

Site classification of the city is calculated based on Nogoshi and Igarashi method (1970, 1971) which is a common classification for microtremor analysis. The basis of this classification is fundamental frequency, thus, with regard to the obtained frequencies, ground type of Meybod is achieved that it has shown in Table 3 and Fig. 9.

Comparison between the *C–A* fractal model and Nogoshi classification shows that the thresholds obtained by the both methods are similar (Table 4). Indeed it can be said that by frequency separation resulted from fractal *C–A* model, we can identify data minor anomalies and consequently classify site effect results more accurately. Therefore, by this approach other results due to frequency, can be classified and then every category attributed to one specific ground type.

By comparing the soil zonation maps, it is obvious that there are five categories for amplification and k-g value. Meanwhile, there are four categories due to frequency and ground classification. Generally, the amplification of the city is low because of very low variation in the soil composition. Based on the amplification and k-g values (Table 5) of every frequency category, appropriate quantities of amplification and vulnerability index

NPGD
1, 1133–1161, 2014

in any resulted classes of the *C–A* fractal model were derived (Table 6). Accordingly, amplification and k-g in any frequency category are respectively: lower than 2.7 and lower than 1.2 for frequency between 6.2–8 Hz, lower than 5.4 and lower than 4.2 for frequency 4.9–6.2 and lower than or equal to 10 and 40 for the other both frequency groups.

Based on the results obtained by shear wave velocity calculation in the boreholes and results derived via the *C–A* fractal model, the velocities were correlated with threshold values of the *C–A* model (Table 3).

6 Conclusions

The *C–A* fractal model is a useful approach in geophysical analysis to identify anomalies and geological particulars and this has been proved by numerous studies. Also this method could be appropriate for geophysical distribution analysis due to its fractal nature.

In this study, due to comparing site effect classification of the area based on Nogoshi and Igarashi classification and frequency categorization resulted from the *C–A* fractal model, it is obtained that the *C–A* fractal model is a useful tool to distinguish and classify site effect results, so that category boundaries could be recognized more accurately. Therefore, the results are presented better and more suitable and also we can attribute resulted frequency, amplification and vulnerability index to any site class more confidently. Additionally, the thresholds derived via Nogoshi and Igarashi classification for the region were corrected. Accordingly, four site classes were obtained for the city as follows:

– Category 1 (weak rock, hard soil): frequency between 6.2–8 Hz, amplification lower than 2.7 and vulnerability index lower than 1.2. It exists in some points of the center of the city toward the east.

NPGD
1, 1133–1161, 2014

– Category 2 (stiff soil): frequency between 4.9–6.2 Hz, amplification lower than 5.4 and vulnerability index lower than 4.2. It exists mostly in the central parts of the city.

– Category 3 (moderately soft soil): frequency between 2.4–4.9 Hz, amplification lower than 10 and vulnerability index lower than or equal to 40. It exists in the most parts of the city.

– Category 4 (soft soil): frequency lower than 2.4 Hz, amplification lower than 10 and vulnerability index lower than or equal to 40, similar to category 3. It is scattered in the different parts of the city such as east and SE, west and SW, center and NW of the area.

Acknowledgements. The authors thank Islamic Azad University – South Tehran branch for support of this research. In addition, the authors acknowledge Gholamreza Shoaei (assistant professor at engineering geology group, geology section, Tarbiat Modares University) and Alireza Ashofteh for their remarkable contribution.

References

Afzal, P., Khakzad, A., Moarefvand, P., Rashidnejad Omran, N., Esfan-diari, B., and Fadakar Alghalandis, Y.: Geochemical anomaly separation by multifractal modeling in Kahang (Gor Gor) porphyry system, Central Iran, J. Geochem. Explor., 104, 34–46, 2010.

Afzal, P., Zia Zarifi, A., and Bijan Yasrebi, A.: Identification of uranium targets based on airborne radiometric data analysis by using multifractal modeling, Tark and Avanligh 1 : 50 000 sheets, NW Iran, Nonlin. Processes Geophys., 19, 283–289, doi:10.5194/npg-19-283-2012, 2012.

Agterberg, F. P., Cheng, Q., Brown, A., and Good, D.: Multifractal modeling of fractures in the Lac du Bonnet batholith, Manitoba, Comput. Geosci., 22, 497–507, 1996.

Akamatu, K.: On microseisms in frequency range from 1 c/s to 200 c/s, B. Earthq. Res. I. Tokyo, 39, 23–75, 1961.

Allam, A. M.: An Investigation Into the Nature of Microtremors Through Experimental Studies of Seismic Waves, University of Tokyo, Tokyo, 326 pp., 1969.

NPGD
1, 1133–1161, 2014

Architectural Institute of Japan: Earthquake Motion and Ground Condition, AIJ, Shiba, Minato-ku, Tokyo, Japan, 1993.
Bard, P.-Y.: Microtremor measurements: a tool for site effects estimations?, in: Proceedings of the Second International Symposium on the Effects of Surface Geology on Seismic Motion, December 1998, Yokohama, Japan, 3, 1251–1279, 1998.
Bard, P. Y.: Lecture notes on "Seismology, Seismic Hazard Assessment and Risk Mitigation", International Training Course, Potsdam, 160 pp., 2000.
Beroya, M. A. A., Aydin, A., Tiglao, R., and Lasala, M.: Use of microtremor in liquefaction hazard mapping, Eng. Geol., 107, 140–153, 2009.
Bolviken, B., Stokke, P. R., Feder, J., and Jossang, T.: The fractal nature of geochemical landscapes, J. Geochem. Explor., 43, 91–109, 1992.
Cheng, Q.: Spatial and scaling modelling for geochemical anomaly separation, J. Geochem. Explor., 65, 175–194, 1999.
Cheng, Q.: Mapping singularities with stream sediment geochemical data for prediction of undiscovered mineral deposits in Gejiu, Yunnan Province, China, Ore Geol. Rev., 32, 314–324, 2007.
Cheng, Q., Agterberg, F. P., and Ballantyne, S. B.: The separartion of geochemical anomalies from background by fractal methods, J. Geochem. Explor., 51, 109–130, 1994.
Daneshvar Saein, L., Rasa, I., Rashidnejad Omran, N., Moarefvand, P., and Afzal, P.: Application of concentration-volume fractal method in induced polarization and resistivity data interpretation for Cu-Mo porphyry deposits exploration, case study: Nowchun Cu-Mo deposit, SE Iran, Nonlin. Processes Geophys., 19, 431–438, doi:10.5194/npg-19-431-2012, 2012.
Davis, J. C.: Statistics and Data Analysis in Geology, 3rd Edn., John Wiley & Sons Inc., New York, 638 pp., 2002.
Douze, E. J.: Rayleigh waves in short period seismic noise, B. Seismol. Soc. Am., 54, 1197–1212, 1964.
Duval, A. M.: Détermination de la Résponse d'un Site aux Séismes á l'Aide du Bruit de Fond: Évaluation Expérimentale, Ph.D. thesis, Université Pierre et Marie Curie, Paris, 1994.
Duval, A.-M.: Détermination de la Réponse d'un Site aux Séismes à l'Aide du Bruit de Fond, Evaluation Expérimentale, Etudes et Recherches des Laboratories des Ponts et Chaussées, Série Géotechnique, Laboratoire central des ponts et chausseées, Paris, 264 pp., 1996.

NPGD
1, 1133–1161, 2014

Evertz, C. J. G. and Mandelbrot, B. B.: Multifractal measures (appendix B), in: Chaos and Fractals, edited by: Peitgen, H.-O., Jurgens, H., and Saupe, D., Springer, New York, 953 pp., 1992.
Gettings, M. E.: Multifractal magnetic susceptibility distribution models of hydrothermally altered rocks in the Needle Creek Igneous Center of the Absaroka Mountains, Wyoming, Nonlin. Processes Geophys., 12, 587–601, doi:10.5194/npg-12-587-2005, 2005.
Goncalves, M. A.: Characterization of geochemical distributions using multifractal models, Math. Geol., 33, 41–61, 2001.
Goncalves, M. A., Mateus, A., and Oliveira, V.: Geochemical anomaly separation by multifractal modeling, J. Geochem. Explor., 72, 91–114, 2001.
Gosar, A. and Roser, J.: Microtremor study of site effects and soil-structure resonance in the city of Ljubljana (central Slovenia), B. Earthq. Eng., 8, 571–592, 2010.
Gosar, A., Stoper, R., and Roser, J.: Comparative test of active and passive multichannel analysis of surface waves (MASW) methods and microtremor HVSR method, RMZ Material and Geo-environment, 55, 41–66, 2008.
Guest, B., Axen, G. J., Lam, P. S., and Hassanzadeh, J.: Late Cenozoic shortening in the west-central Alborz Mountains, northern Iran, Geosphere, 2, 35–52, 2006.
Halsey, T. C., Jensen, M. H., Kadanoff, L. P., Procaccia, I., and Shraiman, B. I.: Fractal measures and their singularities: the characterization of strange sets, Phys. Rev. A, 33, 1141–1151, 1986.
Heidari, S. M., Ghaderi, M., and Afzal, P.: Delineating mineralized phases based on lithogeochemical data using multifractal model in Touzlar epithermal Au-Ag (Cu) deposit, NW Iran, Appl. Geochem., 31, 119–132, 2013.
Kamalian, M., Jafari, M. K., Ghayamghamian, M. R., Shafiee, A., Hamzehloo, H., Haghshenas, E., and Sohrabi-bidar, A.: Site effect microzonation of Qom, Iran, Eng. Geol., 97, 63–79, 2008.
Kanai, K. and Tanaka, T.: Measurement of the microtremor, B. Earthq. Res. I. Tokyo, 32, 199–209, 1954.
Komak Panah, A., Hafezi Moghaddas, N., Ghayamghamian, M. R., Motosaka, M., Jafari, M. K., and Uromieh, A.: Site effect classification in east-central of Iran, J. Seismol. Earthq. Eng., 4, 37–46, 2002.

NPGD
1, 1133–1161, 2014

Konno, K. and Ohmachi, T.: ground motion characteristics estimated from spectral ratio between horizontal and vertical components of microtremor, B. Seismol. Soc. Am., 88, 228–241, 1998.
Lima, A., De Vivo, B., Cicchella, D., Cortini, M., and Albanese, S.: Multifractal IDW interpolation and fractal filtering method in environmental studies: an application on regional stream sediments of (Italy), Campania region, Appl. Geochem., 18, 1853–1865, 2003.
Mandelbrot, B. B.: The Fractal Geometry of Nature, W. H. Freeman, San Fransisco, 468 pp., 1983.
Mukhopadhyay, S. and Bormann, P.: Low cost seismic microzonation using microtremor data: an example from Delhi, India, J. Asian Earth Sci., 24, 271–280, 2004.
Nakamura, Y.: A method for dynamic characteristics estimation of subsurface using microtremore on the ground surface, Quarterly report of Railway Technical Res. Inst. – RTRI, 30-1, 25–33, 1989.
Nakamura, Y.: Real-time information systems for hazard mitigation, in: Proceedings of the 10th World Conference in Earthquake Engineering, Paper #2134, Anchorage, Alaska, 1996.
Nogoshi, M. and Igarashi, T.: On the propagation characteristics of microtremors, J. Seismol. Soc. Jpn., 23, 264–280, 1970.
Nogoshi, M. and Igarashi, T.: On the amplitude characteristics of microtremor (Part 2), J. Seismol. Soc. Jpn., 24, 26–40, 1971.
SESAME: Guidelines for the implementation of the *H/V* spectral ratio technique on ambient vibrations: measurements, processing and interpretation, available at: http://sesamefp5.obs.ujf-grenoble.fr/Delivrables/Del-D23HV_User_Guidelines.pdf, last access: July 2011, 62 pp., 2004.
Sim, B. L., Agterberg, F. P., and Beaudry, C.: Determining the cutoff between background and relative base metal contamination levels using multifractal methods, Comput. Geosci., 25, 1023–1041, 1999.
Turcotte, D. L.: A fractal approach to the relationship between ore grade and tonnage, Econ. Geol., 18, 1525–1532, 1986.
Turcotte, D. L.: Fractals and Chaos in Geology and Geophysics, Cambridge University Press, Cambridge, 1997.

NPGD
1, 1133–1161, 2014

Table 1. Site effect classification of Komak Panah et al. (2002).

Geological Condition	V_s^{30} ($m\,s^{-1}$)	Predominant frequency (Hz)	Soil description	Class no.
Thick soft clay or silty sandy clay mostly alluvial plain	< 350	< 2.5	soft soil	I
Interbeded of fine and coarse material, alluvium terraces with weak cementation	350–550	2.5–5	moderately soft soil	IIa
Thick old alluvium terraces or colluviums soils with medium to good cementation	550–750	5–7.5	stiff soil	IIb
Well cemented and compacted soil, old quaternary outcrop	> 750	> 7.5	hard soil, weak rock	III

NPGD
1, 1133–1161, 2014

Table 2. Site effect classification of Nogoshi and Igarashi (1970).

Description	Frequency (Hz)	Type
Stiff rock composed of gravel, sand and other soils mainly consisting of tertiary or older layers	7–10	I
Sandy gravel, stiff sandy clay, loam or sandy alluvial deposits whose depths are 5 m or greater	4.5–7	II
Standard grounds other than type I, II or IV	2–4.5	III
Soft alluvium-delta lands and pit whose depth is 20 m or greater. Reclaimed land from swamps or muddy shoal where the ground depth is 2 m or greater and less than 20 years have passed since the reclamation.	0/1–2	IV

NPGD
1, 1133–1161, 2014

Table 3. Velocity of seismic waves ($m\,s^{-1}$) in the Meybod city.

Borehole	B.H1		B.H2		B.H3		B.H4		B.H5	
V_p	V_s	V_p	V_s	V_p	V_s	V_p	V_s	V_p	V_s	Depth (m)
1.0	243	567	308	659	217	477	157	353	352	782
2.0	329	743	356	759	283	615	225	501	415	905
4.0	441	961	440	936	360	784	311	685	520	1100
6.0	505	1081	464	997	407	882	377	820	548	1155
8.0	532	1132	487	1045	451	968	405	881	561	1177
10.0	521	1121	505	1080	473	1015	428	927	568	1192
12.0	517	1121	523	1114	503	1070	449	969	592	1231
14.0	505	1108	537	1141	525	1111	476	1019	612	1262
16.0	490	1086	551	1164	525	1118	494	1053	625	1286
18.0	493	1093	564	1188	528	1130	507	1078	628	1292
20.0	497	1097	573	1207	535	1142	506	1081	643	1316
22.0	503	1108	585	1228	550	1169	512	1094	651	1330
24.0	509	1119	595	1244	562	1190	522	1113	662	1345
26.0	518	1135	602	1256	575	1211	525	1121	672	1361
28.0	526	1149	605	1263	585	1227	532	1134	683	1377
30.0	534	1163	609	1271	592	1240	543	1152	692	1390
32.0	539	1169	616	1283	601	1254	552	1168	700	1403
34.0	541	1172	624	1295	603	1259	562	1184	703	1411
36.0	545	1176	631	1306	610	1269	571	1197	708	1419
38.0	551	1185	637	1315	617	1280	577	1208	714	1428
40.0	555	1192	644	1325	623	1291	581	1215	719	1436
42.0	559	1199	650	1335	629	1301	588	1226	725	1444
V_s^{30} ($m\,s^{-1}$)	473		509		460		407		579	
seismic bed rock depth (m)	70		90		80		80		52	

NPGD
1, 1133–1161, 2014

Table 4. Comparison of frequency separation by *C–A* fractal model and Nogoshi and Igarashi (1970, 1971).

Nogoshi		*C–A* fractal model	
Frequency (Hz)	Ground type	Frequency (Hz)	Category
7–10	I	6.2–8	4
4.5–7	II	4.9–6.2	3
2–4.5	III	2.4–4.9	2
0.1–2	IV	0–2.4	1

NPGD
1, 1133–1161, 2014

Table 5. Frequency of amplification and k-g classes in every frequency category.

Frequency	Amplification classes					k-g classes				
Classes (Hz)	< 1.6	1.6–2.7	2.7–5.4	5.4–6	6–10	< 1.2	1.2–4.2	4.2–10	10–19	19–40
6.2–8	4	10	0	0	0	14	0	0	0	0
4.9–6.2	15	5	2	0	0	19	3	0	0	0
2.4–4.9	22	21	12	2	2	28	25	3	1	2
< 2.4	28	18	18	0	1	20	24	16	3	2

NPGD
1, 1133–1161, 2014

Table 6. Site effect classification based on *C–A* method.

Site description	Frequency (Hz)	Amplification	k-g
hard soil, weak rock	6.2–8	< 2.7	< 1.2
stiff soil	4.9–6.2	< 5.4	< 4.2
moderately soft soil	2.4–4.9	< 10	≤ 40
soft soil	0–2.4	< 10	≤ 40

NPGD
1, 1133–1161, 2014

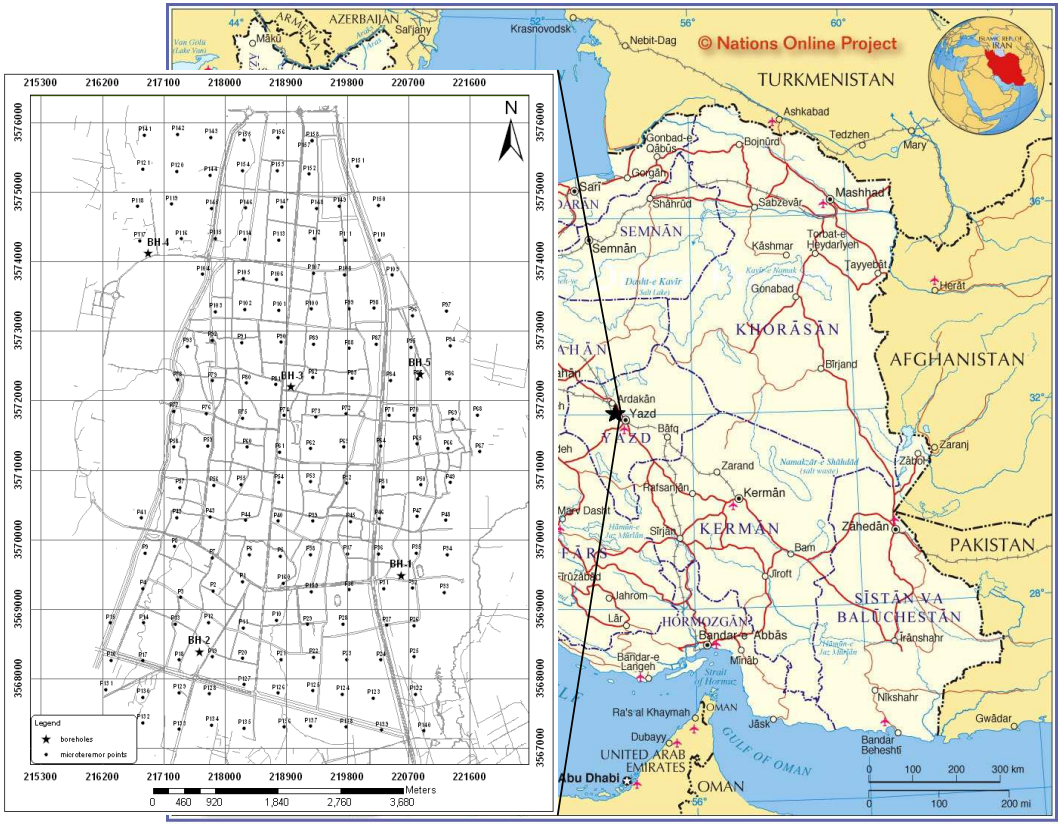

Figure 1. The political map of Iran (the Nations Online Project); the location of the study area (shown by a black star), and the microtremor recording points and boreholes map.

NPGD
1, 1133–1161, 2014

Site effect classification based on microtremor data analysis

A. Adib et al.

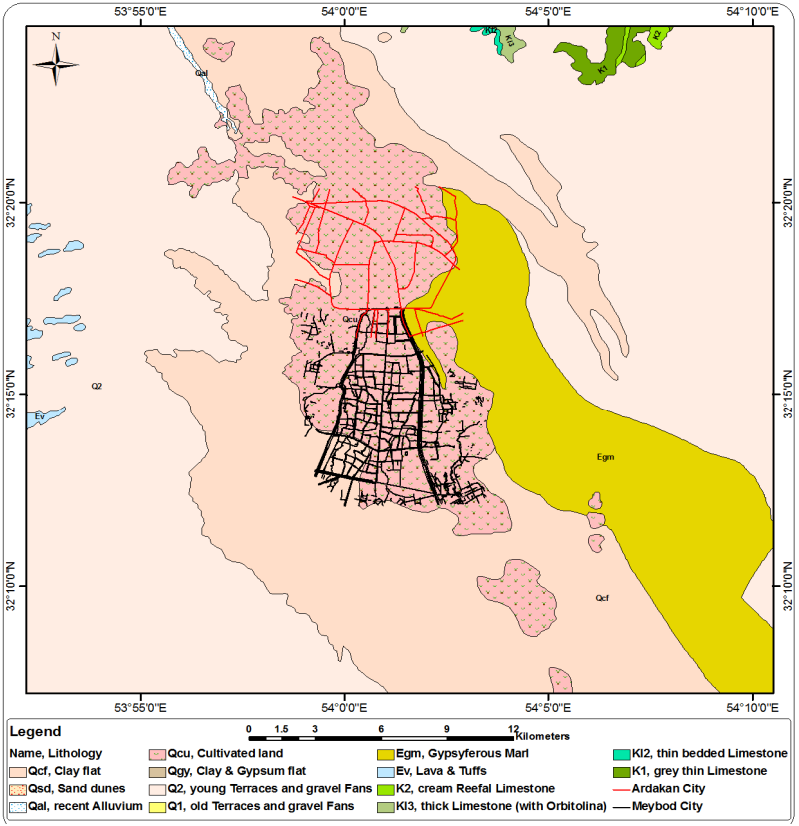

Figure 2. Geological map around Meybod city. According to the map, the major units around the city are Quaternary deposits including cultivated land, Clay flat and young terraces and fans. The only other unit that is close to the city is Eocene gypsiferous Marls (Egm).

NPGD
1, 1133–1161, 2014

Site effect classification based on microtremor data analysis

A. Adib et al.

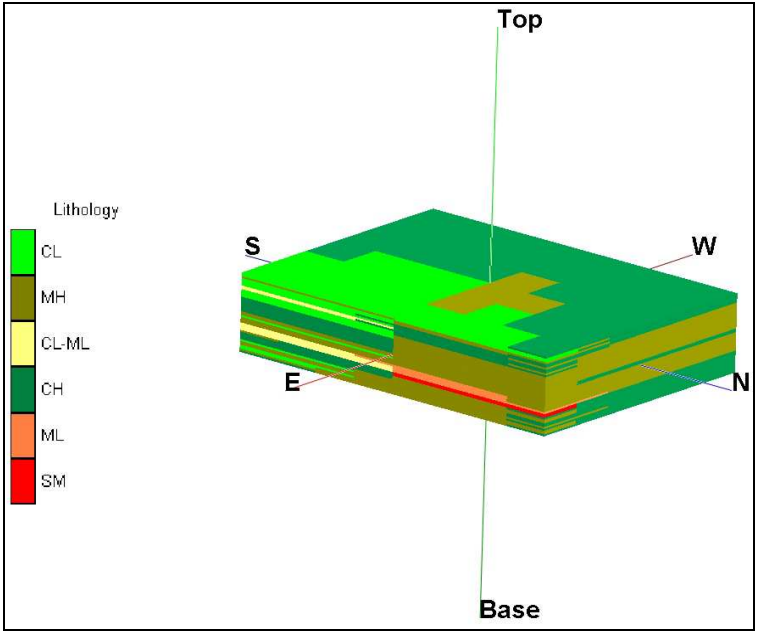

Figure 3. 3-D model of soil deposits of Meybod city, Iran. Dominant soil type is composed of clay and silt with high plasticity. The major variation is located in the eastern part of the city (CL: inorganic clay of low plasticity or lean clay; MH: inorganic silt of high plasticity; CL-ML: inorganic clay and inorganic silt of low plasticity; CH: inorganic clay of high plasticity; ML: inorganic silt of low plasticity; SM: silty sand).

NPGD
1, 1133–1161, 2014

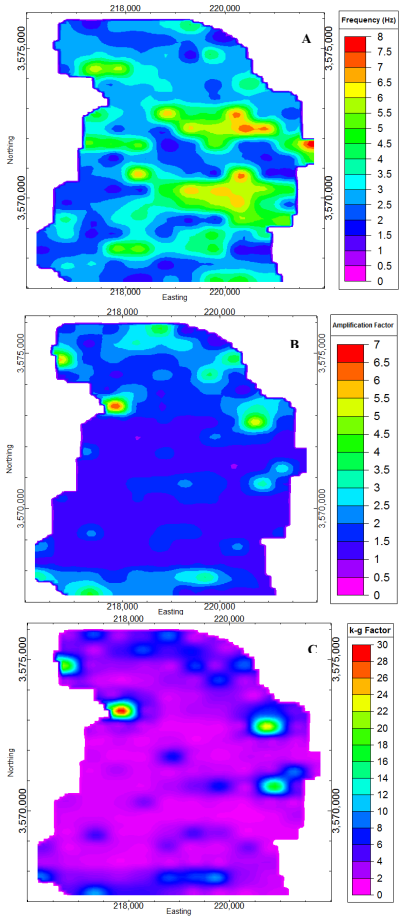

Figure 4. Data distribution maps in the Meybod city: **(A)** frequency; **(B)** amplification; **(C)** k-g value.

NPGD
1, 1133–1161, 2014

Site effect classification based on microtremor data analysis

A. Adib et al.

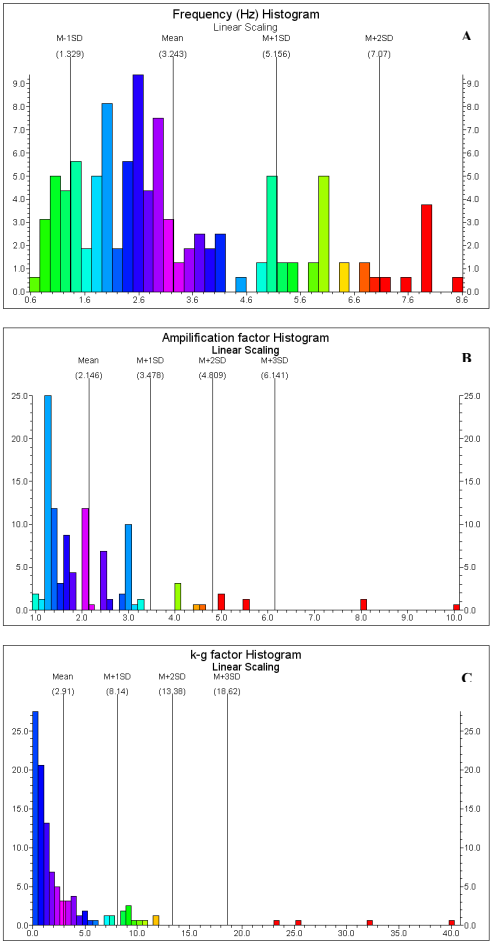

Figure 5. Data histograms show multimodality of the factors. **(A)** Frequency, **(B)** amplification, **(C)** k-g value.

NPGD
1, 1133–1161, 2014

Site effect classification based on microtremor data analysis

A. Adib et al.

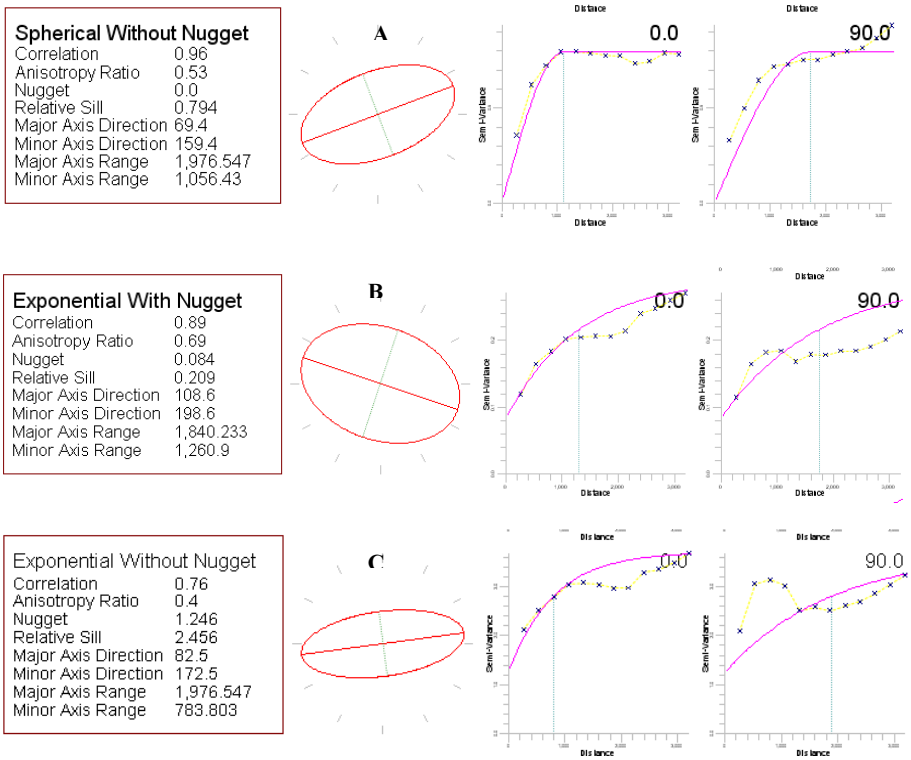

Figure 6. Variograms and anisotropic elipsoids of the parameters: **(A)** frequency; **(B)** amplification; **(C)** k-g value.

NPGD
1, 1133–1161, 2014

Site effect classification based on microtremor data analysis

A. Adib et al.

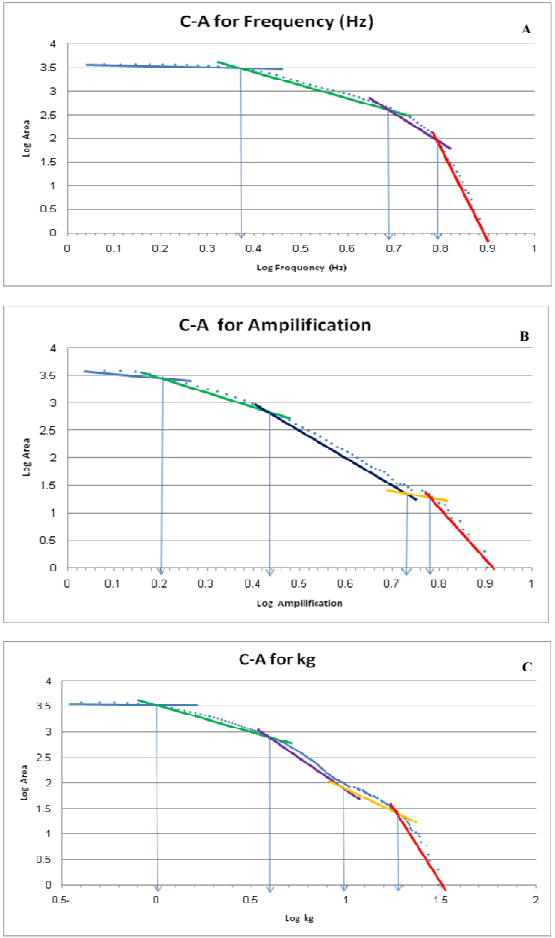

Figure 7. *C–A* log–log plot for the parameters: **(A)** frequency, **(B)** amplification, **(C)** k-g value.

NPGD
1, 1133–1161, 2014

Site effect classification based on microtremor data analysis

A. Adib et al.

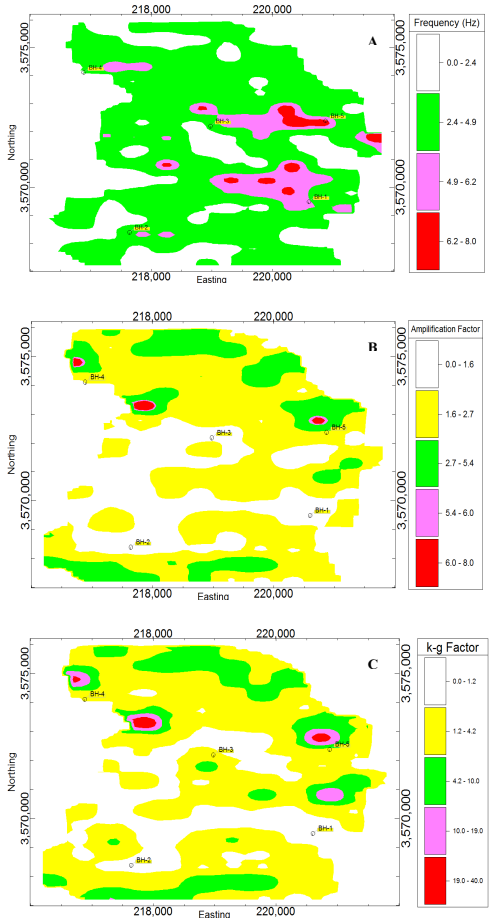

Figure 8. Data classification based on *C–A* method. **(A)** frequency, **(B)** amplification, **(C)** k-g value.

NPGD
1, 1133–1161, 2014

Site effect classification based on microtremor data analysis

A. Adib et al.

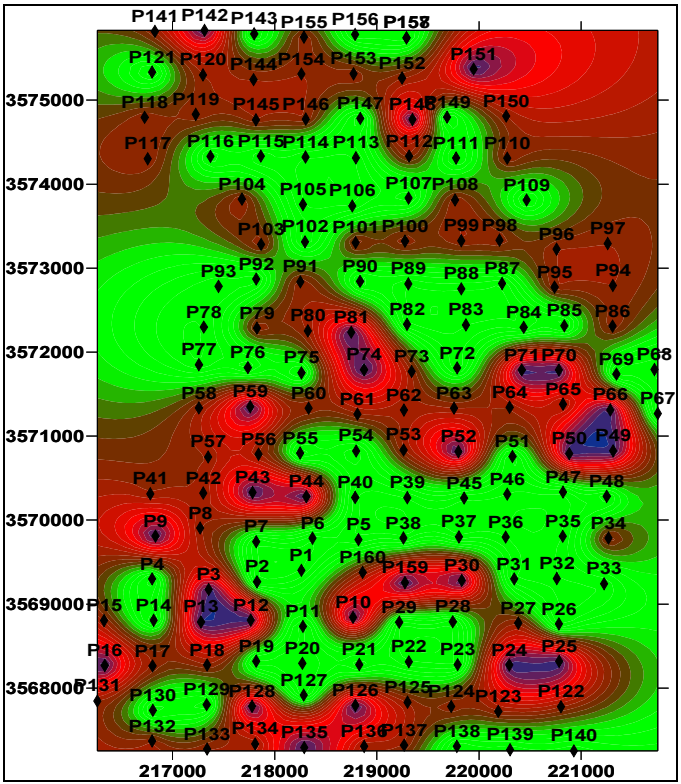

Figure 9. Ground type zonation of the region based on Nogoshi and Igarashi (1970, 1971). Violet color (points 12, 13, 24, 25, 49, 50, 74 and 151) is ground type 4; (dark) red color represents type 3 and (light) green color is type 2.

NPGD
1, 1133–1161, 2014

Site effect classification based on microtremor data analysis

A. Adib et al.